



HAL
open science

Treatment of human pancreatic cancer using combined ultrasound, microbubbles, and gemcitabine: a clinical case study

Spiros Kotopoulos, Georg Dimcevski, Odd Helge Gilja, Dag Hoem, Michiel Postema

► **To cite this version:**

Spiros Kotopoulos, Georg Dimcevski, Odd Helge Gilja, Dag Hoem, Michiel Postema. Treatment of human pancreatic cancer using combined ultrasound, microbubbles, and gemcitabine: a clinical case study. *Medical Physics: The international journal of medical physics research and practice*, 2013, 40 (7), pp.072902. <10.1118/1.4808149>. <hal-03193216>

HAL Id: hal-03193216

<https://hal.science/hal-03193216v1>

Submitted on 16 Apr 2021

HAL is a multi-disciplinary open access archive for the deposit and dissemination of scientific research documents, whether they are published or not. The documents may come from teaching and research institutions in France or abroad, or from public or private research centers.

L'archive ouverte pluridisciplinaire **HAL**, est destinée au dépôt et à la diffusion de documents scientifiques de niveau recherche, publiés ou non, émanant des établissements d'enseignement et de recherche français ou étrangers, des laboratoires publics ou privés.



HAL Authorization

1 **Treatment of human pancreatic cancer using combined ultrasound,**
2 **microbubbles and gemcitabine: a clinical case study.**

3 Spiros Kotopoulos^{1,2*}, Georg Dimcevski^{1,3}, Odd Helge Gilja^{1,3}, Dag Hoem⁴, Michiel
4 Postema^{2,5}

5 ¹ National Centre for Ultrasound in Gastroenterology, Haukeland University Hospital, Bergen,
6 Norway

7 ² Department of Physics and Technology, University of Bergen, Bergen, Norway

8 ³ Department of Clinical Medicine, University of Bergen, Bergen, Norway

9 ⁴ Department of Surgery, Haukeland University Hospital, Bergen, Norway

10 ⁵ The Michelsen Centre for Industrial Measurement Science and Technology, Bergen,
11 Norway

12

13 **Abstract**

14 Purpose: The purpose of this study was to investigate the ability and efficacy of
15 inducing sonoporation in a clinical setting, using commercially available technology,
16 to increase the patients' quality of life and extend the low ECOG performance grade;
17 as a result increasing the overall survival in patients with pancreatic adenocarcinoma.

18 Methods: Patients were treated using a customised configuration of a commercial
19 clinical ultrasound scanner over a time period of 31.5 min following standard
20 chemotherapy treatment with gemcitabine. SonoVue[®] ultrasound contrast agent was
21 injected intravascularly during the treatment with the aim to induce sonoporation.

22 Results: Using our custom acoustic settings, our patients were able to undergo an
23 increased number of treatment cycles; from an average of 9 to 16 cycles when

* Corresponding author email: Spiros.Kotopoulos@uib.no

24 comparing to a historical control group of 80 patients. In two out of five patients
25 treated, the maximum tumour diameter was temporally decreased to $80\pm 5\%$ and
26 permanently to $70\pm 5\%$ of their original size, whilst the other patients showed reduced
27 growth.

28 We also explain and characterise the settings and acoustic output obtained from a
29 commercial clinical scanner used for combined ultrasound microbubble and
30 chemotherapy treatment.

31 Conclusion: It is possible to combine ultrasound, microbubbles, and chemotherapy in
32 a clinical setting using commercially available clinical ultrasound scanners to increase
33 the number of treatment cycles, prolonging the quality of life in patients with
34 pancreatic adenocarcinoma compared to chemotherapy alone.

35 **Purpose**

36 Cancer is the world's second largest cause of death with over 7.6 million deaths a year
37 (21% of NCD deaths) [1]. There are over 217 000 new cases of pancreatic cancer
38 worldwide every year [2]. Pancreatic cancer is very difficult to treat due to its
39 aggressive biology, late diagnosis, the encasement of large blood vessels, and the
40 presence of metastasis. Hence, surgery is rarely an option. Chemotherapy produces
41 modest responses but is not curative in this setting, mainly because its use is severely
42 hampered by toxic effects to vital organs. As a result, the survival is very low. The
43 mortality of the inoperable patients is 50% within 3 months and 90% within 12
44 months [3, 4].

45 Sonoporation is a novel method for non-invasive targeted drug and gene delivery [5-
46 8]. Sonoporation is defined as the transient formation of pores in cell membranes
47 owing to ultrasound or a combination of ultrasound and microbubbles. These pores
48 range in size from several nanometres to several micrometres [9-12], allowing for
49 increased drug uptake in highly targeted regions [13-15].

50 The acoustic parameters used for sonoporation showing increased cellular uptake of
51 chemotherapeutics and genes vary from low-intensity diagnostic ultrasound
52 (Mechanical Index (MI) < 0.3) [16-29] to high-intensity diagnostic ultrasound (MI >
53 1.0) [9, 30-34]. Throughout literature, the acoustic settings used to induce
54 sonoporation vary drastically, with a broad range of these settings showing improved
55 drug and gene delivery. Several studies also show the effect of clinical diagnostic
56 ultrasound in standard colour-Doppler and B-mode imaging on cellular uptake [19,
57 20]. These studies, which made use of clinical diagnostic scanners, concluded that a
58 larger duty cycle was necessary to increase the effect of sonoporation. It has been

59 shown that the ideal settings to induce sonoporation are when shock-waves were not
60 present, in order to sustain the microbubbles, and when the duty cycle is long enough,
61 to excite the microbubbles in the targeted area without heating the surrounding tissue
62 [16]. Furthermore, higher intensities correlating to cavitation and jetting result in
63 increased cell death due to mechanical damage instead of (transient) sonoporation [33,
64 35-37]. As a result, there is no consensus on the exact ultrasound settings to be used
65 for sonoporation [38]. For this reason we aimed to use settings that matched our
66 previous *in-vitro* and *in-vivo* work as much as possible, *i.e.*, an *in-situ* MI=0.2,
67 maximum duty cycle, and minimum shockwave generation in order to preserve the
68 microbubbles [7, 8, 23].

69 To date, all sonoporation experiments have been done either *in vitro* or in animal
70 models, hence the effect of sonoporation in humans is not truly known yet.

71 Ultrasound has been used as a tool in the clinic for many years, especially in
72 transabdominal imaging. Specifically, the pancreas can easily be imaged
73 ultrasonically [39]. In clinical ultrasonic imaging, ultrasound is combined with so-
74 called ultrasound contrast agents to locate tumours [40, 41]. These agents consist of
75 gas microbubbles encapsulated by elastic shells [42]. Using a clinical diagnostic
76 scanner for combined imaging and treatment allows for precise acoustic field
77 alignment ensuring that the correct ultrasound intensity reaches the target area.

78 In this study, we worked towards optimising the ultrasonic settings for invoking
79 sonoporation in the target region of a pancreatic tumour using a common commercial
80 clinical ultrasound scanner without physical modifications.

81

82 **Methods**

83 A clinical scanner was calibrated in a degassed water bath in order to map the beam
84 profile and optimise the acoustic settings. After the chemotherapeutic dose was
85 delivered, the clinical probe was positioned aiming directly at the pancreatic tumour
86 and locked in place for 31.5 minutes. The probe was attached to a ball joint and was
87 positioned near the upper abdomen. Stomach and intestine were avoided in all cases
88 to ensure propagation only through soft tissue, to ensure delivery of the aimed
89 ultrasound intensity at the desired area. Once the tumour was located the probe
90 orientation was fine-tuned in order to locate the largest slice of the tumour and as
91 much vasculature as possible, *i.e.*, the feeding vessels. The probe was then locked in
92 position until the completion of the treatment. The natural breathing motion aided the
93 treatment as the ultrasound slice gently oscillated through the tumour. By visualising
94 the vasculature and tumour it could be ensured that the microbubbles were being
95 sonicated at the target. These vessels were then used as a reference point for future
96 treatments. Nine doses of ultrasound contrast agent were intravenously injected over
97 this time period to enhance the sonoporation effect. To evaluate the efficacy of the
98 combined treatment we compared the amount of chemotherapy cycles the patient was
99 able to receive. Furthermore, the tumour size was measured over the course of the
100 treatment cycles to monitor and compare the tumour growth.

101

102 **Ultrasound scanner configuration**

103

104 A GE LOGIQ 9 ultrasound scanner (GE Healthcare, Waukesha, WI) combined with a
105 4C curvilinear probe (GE Healthcare) was used for both diagnosis and therapy.

106 To calibrate and program the diagnostic scanner for the optimised therapeutic settings
107 the probe was locked in position in a custom-made 250-L 3D scanning tank,
108 containing degassed water. A calibrated HGL-200 bullet-type hydrophone (Onda,
109 Sunnyvale, CA) connected to a WaveJet 354a oscilloscope (Teledyne LeCroy SA,
110 Geneva, Switzerland) was used to measure the acoustic signal. The scanning tank had
111 a spatial resolution of 0.4 μm . For the calibration a 200- μm resolution was used.
112 AQUASONIC® ultrasound transmission gel (Parker Laboratories, Fairfield, NJ) was
113 placed on the transducer transmission surface and the probe was subsequently covered
114 using a latex ultrasound probe cover (Sheathing Technologies, Inc., Morgan Hill, CA)
115 prior to submersion. The diagnostic scanner settings were modified in order to
116 achieve a maximum duty cycle without completely degrading the image quality, in
117 addition to having a linear acoustic signal. We aimed for minimal acoustic
118 shockwaves and harmonics minimising potential cavitation. The absence of nonlinear
119 content was verified by visualising the temporal extent of the pulses and performing a
120 Fast Fourier Transform (FFT) [43]. Multiple focal depths (from 2.8 cm to 8.4 cm) and
121 different settings (varying gain, changing window size, etc.) were evaluated to ensure
122 similar acoustic conditions in all cases. To calculate the *in-situ* acoustic pressures and
123 intensities, the *in-water* values were derated by 0.3 dB/MHz/cm, an approximation of
124 soft tissue attenuation in accordance to FDA and IEC guidelines [44, 45]. The
125 attenuation factor of 0.3 dB/MHz/cm is only valid for soft tissue. Hence, this
126 calibration was representative for our clinical positioning for targeting the pancreas.

127

128 Table 1 shows the ultrasound scanner settings used to perform the simultaneous
129 observation and treatment of the pancreatic tumours. Skilled clinical sonographers
130 were called upon to judge the image quality. As there are variations between patients,

131 such as tumour depth and tissue attenuation, certain settings had to be adjusted to
 132 ensure the correct ultrasound intensity reached the required area whilst maintaining
 133 the image quality. The settings that were varied are labelled as *Patient-dependent*.
 134 The three settings that were adjusted prior to treatment were: the focal depth, image
 135 depth, and gain. The focal and image depths were adjusted in order to visualise and
 136 position the acoustic focus directly in the middle of the tumour. By doing so we
 137 could ensure that the acoustic conditions the tumour received was as similar as
 138 possible in all patients. The gain is only applied after the received signal, hence it did
 139 not affect the acoustic output. The gain simply allowed for a brighter image.
 140 Once the probe was locked in position and the tumour was “targeted”, no changes to
 141 the ultrasonic conditions were made.

142
 143

	B-mode	Contrast mode			
Parameter	Value		Unit	Description	Variability
MI	0.4	0.4		Mechanical Index	None
TIs	0.0	0.0		Thermal Index of soft tissue	None
Freq	4.0	4.0	MHz	Centre Receive frequency	None
AO	1	36	%	Normalised acoustic output	None
FR	4	4	fps	Frame rate	None
Gn	30-45	30-45	dB	Gain	Patient-dependent
S/A	3/3	2/0		Synthetic Aperture	None
Map	F/0	2/0		Colour map	None
F	5.2-6.8	5.2-6.8	cm	Focal depth	Patient-dependent
D	10-15	10-15	cm	Image Depth	Patient-dependent
DR	66	66	dB	Dynamic Range	None
SRI HD	3	3		Image smoothing	None
Grey Map	F/0	H		Image colour maps	None

Trig	-0.25	-	s	Trigger delay	None
Tint Map	D	-		Image colour maps	None
Trig	-	0-1		Image triggering	None
TAD	-	on		True Agent Detection	None
F.Average	-	3	frames	Frame averaging	None

144 **Table 1:** Parameters as indicated on a GE LOGIQ 9 clinical ultrasound scanner.

145 The settings chosen resulted in acoustic conditions shown in Table 2 and beam
 146 profiles shown in Figure 1.

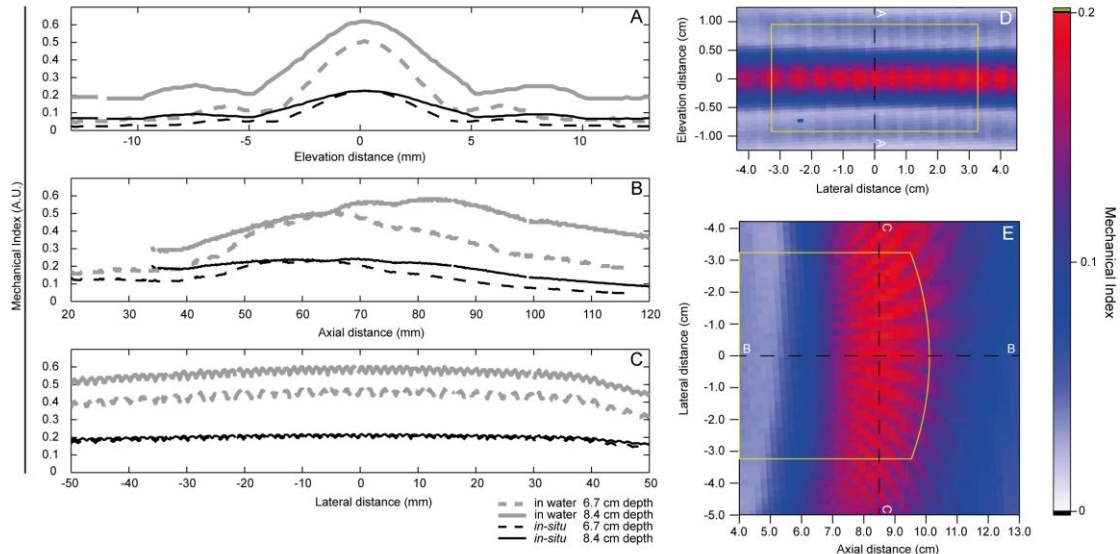
147

	Centre frequency (MHz)	Duty cycle (%)	Mechanical Index	Acoustic power I_{SATA} (mW/cm ²)	Peak peak-negative acoustic pressure (MPa)
<i>in-water</i> values at 6.7 cm depth	1.9	1 (4 cycles every 0.21 ms)	0.49	0.59	0.41
Derated <i>in-situ</i> values at 6.7 cm depth	1.9	1 (4 cycles every 0.21 ms)	0.20	0.25	0.27

148

149 **Table 2:** Acoustic conditions generated by the 4C probe for sonoporation *in-water*
 150 and derated for *in-situ* values [44, 45].

151



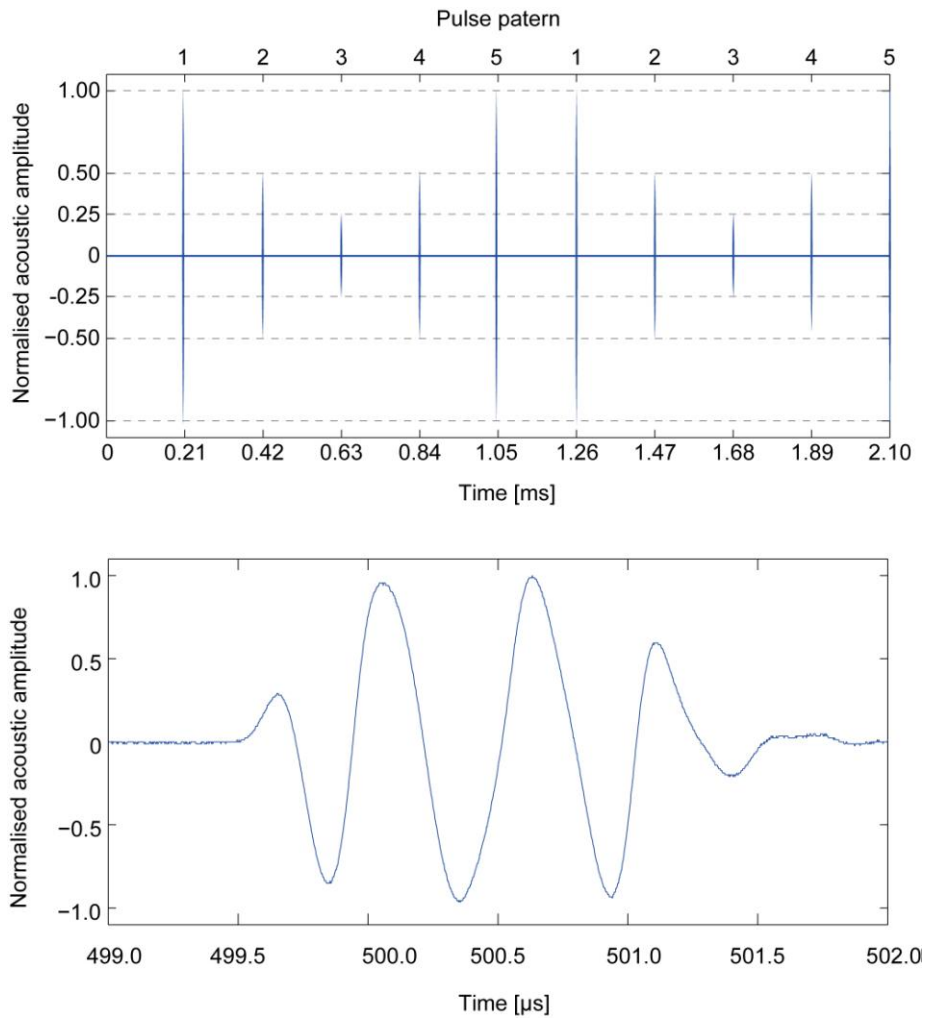
152

153 **Figure 1:** 1D and 2D beam profiles at sonoporation settings using the 4C probe at two
 154 focal depths: 6.7 cm and 8.4 cm for the 1D plots and 8.4 cm for the 2D plots. The
 155 beam profile was characterised in water and derated for *in-situ* values [44, 45]. Lines
 156 A-A, B-B, and C-C in panels D and E represent the position of the 1D scans shown in
 157 panels A, B and C respectively. The yellow bounding boxes in panels D and E
 158 represent the area visible on the clinical scanner screen. In the elevation direction the
 159 bounding box was defined by when a 0.5mm needle could not be distinguished on
 160 screen. The tumour was positioned at the intersection of lines B-B and C-C in frame E,
 161 and at an elevation distance of 0 mm in frame D.

162

163 The beam profile showed formation of multiple foci in close proximity along the
 164 lateral direction merging to form a quasi-continuous focus (Figure 1E). In the
 165 elevation direction side lobes can be clearly seen (Figure 1A and 1D). Using the full
 166 width half maximum (FWHM) to define the beam size, the active or treatment area
 167 can be defined as a volume of $69 \times >100 \times 1.0 \text{ (mm)}^3$ ($l \times w \times h$). It is assumed that this
 168 is the region where sonoporation occurred most efficiently. Figure 2 shows the pulse

169 repetition pattern generated by these settings. The pulse was amplitude-modulated,
170 consisting of 5 cycles ($2.1 \mu\text{s}$) every $210 \mu\text{s}$ corresponding to a 1% duty cycle
171 (repetition rate optimised). The duty cycle is defined as the percentage of time that
172 ultrasound is being generated. This was measured during the spatial calibration
173 process, in the acoustic focus with the hydrophone, for the duration of the inverse of
174 the frame rate. Due to synthetic aperture and contrast enhanced imaging the pulse
175 pattern at the focus was amplitude-modulated [46] [47]. This can be seen in the upper
176 panel of Fig. 2. The lower panel of Fig. 2 shows the time signal of a single pulse. The
177 pulse is still relatively sine-shaped, thus the transfer function of the propagation path
178 is linear. Minor nonlinear effects can be seen after the 4th cycle. This indicates that
179 shockwave occurrence and therefore microbubble destruction is negligible.



180

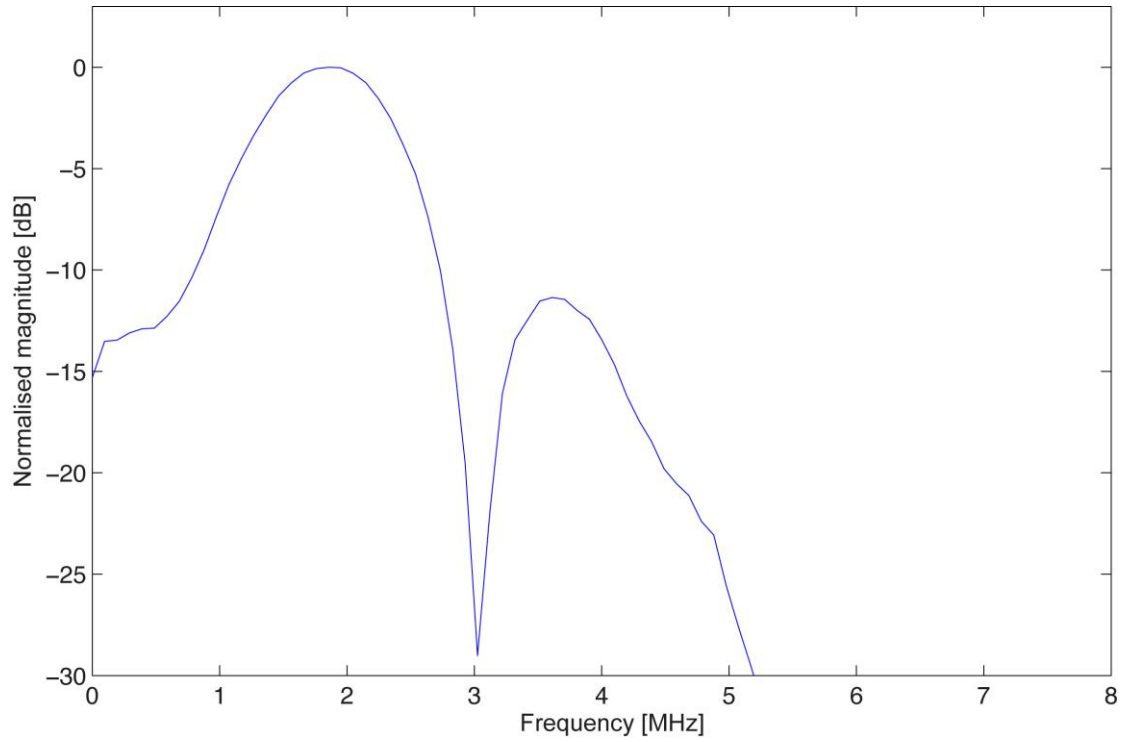
181 **Figure 2:** Ultrasonic pulse generated by the clinical scanner. The top panel shows the
 182 pulse repetition frequency and pattern. The lower panel shows the temporal extent of
 183 the pulse with the largest amplitude. The pulses were amplitude-modulated. Each
 184 pulse consisted of 4 cycles (2.1 μ s) every 210 μ s.

185 A Fast Fourier Transform (FFT) of the acoustic signal is shown in Fig. 3. The centre
 186 frequency is 1.9 MHz. Using a -3 -dB or FWHM cut-off the bandwidth was measured
 187 to be 1.1 MHz; from 1.3 – 2.4 MHz. A second harmonic peak can be seen at 3.6 MHz
 188 due to the minor non-linear effects. This peak was 11 dB lower than the primary peak.

189

190 These settings complied with current safety guidelines for clinical diagnostic imaging
191 [44, 48, 49]. Figure 4 shows two images of pancreatic cancer in two separate patients
192 captured using the sonoporation treatment settings.

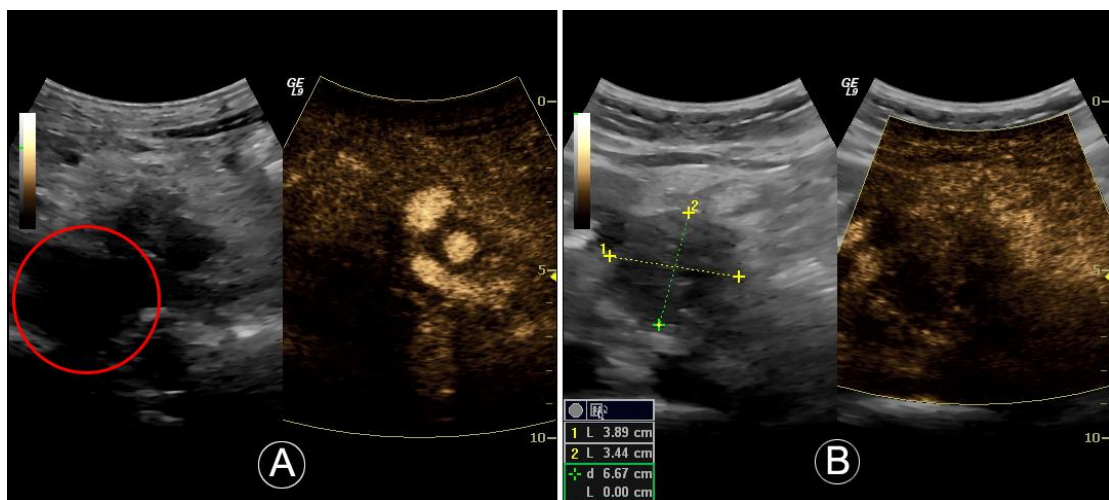
193



194

195 **Figure 3:** Fast Fourier transform of ultrasonic signal. The centre frequency of the
196 transmitted signal is 1.9 MHz. A bandwidth of 1.1 MHz can be seen.

197



198

199 **Figure 4:** Images captured using customised sonoporation settings using a clinical
200 ultrasound scanner. The dense vasculature in early arterial phase to the right of the
201 main tumour (circled in red) can be seen in panel A. Panel B shows the dimensions of
202 the main tumour, indicated by lines 1 and 2, using the sonoporation settings.

203

204 **Chemotherapeutic and Microbubble dosage**

205

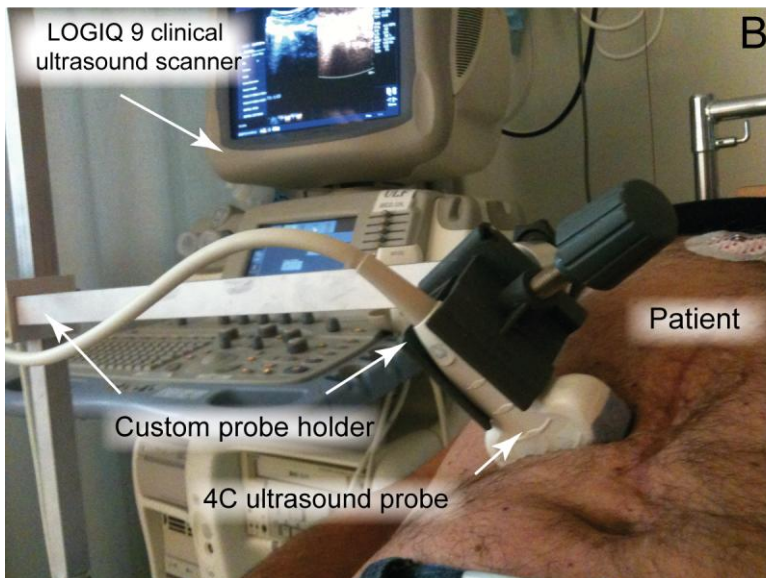
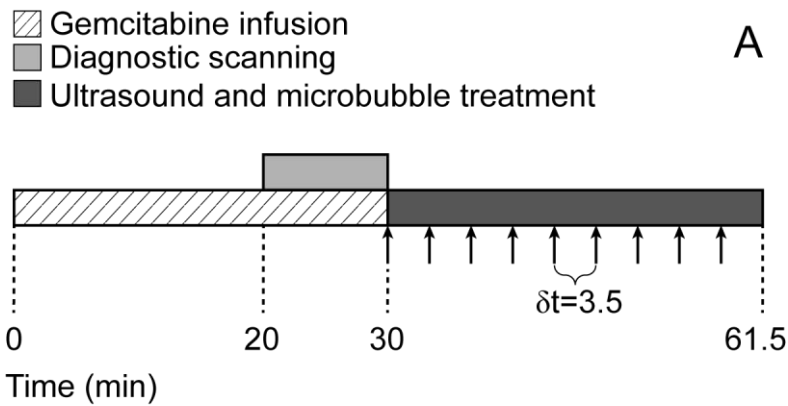
206 The recommended chemotherapeutic protocol was followed [50]. This protocol
207 dictates which patients are eligible for chemotherapy and the dosages that can be
208 administered. It includes dosage reduction values depending on platelet and absolute
209 granulocyte count. The chemotherapeutic used, gemcitabine (Gemzar[®], Eli Lilly and
210 Company, Indianapolis, IN) was administered once weekly for up to 7 weeks (or until
211 toxicity necessitates reducing or holding a dose), followed by a week of rest from
212 treatment. Subsequent cycles consisted of infusions once weekly for 3 consecutive
213 weeks out of every 4 weeks. Our protocol used the Eastern Cooperative Oncology
214 Group (ECOG) performance status as a measure of the clinical condition [51]. The
215 ECOG performance status ranges from 0–5, where 0 denotes a “*fully active patient*
216 *able to carry on all pre-disease performance without restriction*”, and 5 denotes a
217 “*dead*” patient. Chemotherapy was halted if the patient exceeded a grade of 2 that
218 states the patient is “*ambulatory and capable of all self-care but unable to carry out*
219 *any works activities. Up and about more than 50% of waking hours.*” The ECOG
220 guidelines can be considered as a measure of how “healthy” a patient is. We used the
221 ECOG guidelines to monitor the effectiveness of the combined treatment *i.e.*, the
222 longer a patient stays below an ECOG grade of 3, the more effective the treatment is
223 considered.

224 A single treatment cycle is defined as a single infusion of chemotherapeutic followed
225 by ultrasound and microbubble treatment. The week pause was not counted as a
226 treatment cycle. Once the granulocyte or platelet count was permanently too low, or
227 the patient surpassed an ECOG performance status grade of 2, no more treatment was
228 administered.

229

230 Gemcitabine was administered by intravenous infusion at a dose of 1000 mg/m^2 over
231 30 minutes. The start of the chemotherapeutic delivery is defined as $T = 0 \text{ min}$.
232 During the last 10 minutes ($T = 20 \text{ min}$) of chemotherapeutic delivery, diagnostic
233 imaging was performed in standard abdominal imaging mode and the tumour was
234 located. Here the tumour dimensions were measured with ultrasonography. Once the
235 tumour was located, a custom made clamp was used to lock the probe in position and
236 the clinical scanner was switched to therapeutic settings (Fig 5). As the maximum
237 systemic concentration of the chemotherapeutic starts at the finish of delivery
238 ($T = 30 \text{ min}$) this was chosen as the initiation point for the ultrasound treatment.
239 Clinically approved SonoVue[®] (Bracco Imaging Scandinavia AB, Oslo, Norway)
240 ultrasound contrast agent was used as the microbubble for sonoporation. To ensure
241 microbubbles were present throughout the whole treatment 0.5 mL of contrast agent
242 followed by 5 mL saline were injected every 3.5 min, *i.e.*, at
243 $T = 30.0, 33.5, 37.0, 40.5, 44.0, 47.5, 51.0, 54.5$ and 58.0 min . A single vial (4.5
244 mL) was used throughout each treatment. Treatment was stopped at $T = 61.5 \text{ min}$.
245 The total cumulated ultrasound treatment time was only 18.9 s. This time frame can
246 be seen in Fig. 5A.

247



248

249 **Figure 5:** Time frame of each chemotherapy cycle (Panel A) and photograph of probe
 250 and custom made probe holder during patient treatment using microbubble
 251 sonoporation for pancreatic cancer (Panel B). Panel A shows the time frame for each
 252 treatment cycle from the start of the gemcitabine infusion. Arrows indicate
 253 intravenous injection time of 0.5 mL SonoVue[®] followed by a 5-mL intravenous
 254 injection of saline. Time between each injection (δt) is 3.5 minutes.

255

256

257 **Measurement of disease and tumour progression**

258

259 The primary measure for evaluating the effectiveness of the treatment was the amount
260 of cycles the patient could undergo. The more treatment cycles the patient underwent,
261 the longer the patient was considered healthy [50, 51]. Furthermore, if the tumour size
262 was reduced substantially in accordance to the Response Evaluation Criteria in Solid
263 Tumours (RECIST) [52], the treatment modality was re-evaluated, *e.g.* transfer to
264 radiation therapy or surgery. This was considered a successful treatment.

265 Diagnostic ultrasound imaging was performed weekly assessing the tumour size. As
266 Computerised Tomography CT scans are considered the golden standard for
267 following tumour growth [53], every 8 weeks a CT scan was also performed to
268 validate the tumour size. This value was used to follow the tumour progression.

269 Positron Emission Tomography (PET) imaging was also performed at the start of the
270 treatment to assess the presence of metastasis.

271 Figure 6 shows the pancreatic adenocarcinoma in patient 5 prior to ultrasound and
272 microbubble treatment as seen by CT and PET imaging modalities.

273

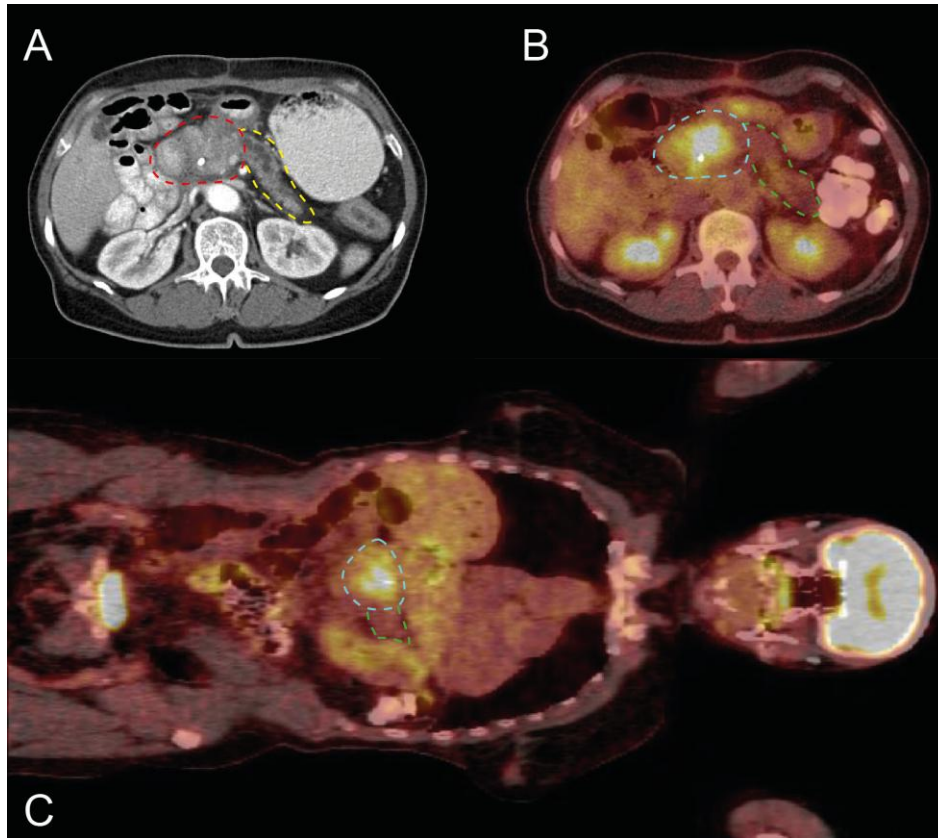


Figure 6. CT (Panel A) and PET (Panels B and C) images of patient 5 showing pancreatic adenocarcinoma prior to treatment. Panel A shows a CT scan in the transverse plane with the primary tumour in the head of the pancreas, and the pancreas indicated by the red and yellow dashed lines respectively. Panels B and C show PET scans in transverse and coronal plane respectively. The location of the tumour can be clearly identified by the brighter colour in the middle of the abdomen. In Panels B and C, the tumour and pancreas are respectively indicated by the blue and green dashed lines. The pancreas tail is behind the large colon in panel C.

274

275 **Treatment group**

276 Patients with inoperable pancreatic cancer and fulfilled the inclusion criteria at the
277 Haukeland University Hospital, Bergen, Norway, who have volunteered to participate,
278 were included. The inclusion criteria primarily stated that the patients must be > 18

279 years of age, a diagnosis of inoperable pancreatic cancer, histologically verified,
 280 locally advanced (stage II/III) or metastatic (stage IV) adenocarcinoma of the
 281 pancreas, and must be ambulatory with an ECOG performance status between 0 and 2.
 282 For this case report a total of five patients were recruited. Table 3 shows the
 283 characteristics of the five patients enrolled in this pilot study prior to treatment in
 284 addition to the start and end dates of the treatment for every patient.

		Patient 1	Patient 2	Patient 3	Patient 4	Patient 5
Age		66	55	70	68	51
Sex		Male	Male	Female	Female	Female
Pathology Findings		Pancreatic ductal adenocarcinoma				
ECOG Performance		0	1	1	0	1
Biochemistry	ALAT IU/L	20	55	138	23	66
	LD IU/L	121	146	153	117	176
	Leuk $\times 10^9$ U/L	6.8	3.8	6.9	6.1	11.1
	Neutr $\times 10^9$ U/L	4.3	5.8	3.8	3.5	7.1
Tumour Markers	Ca 125	ND	54.1	102	ND	136.6
	Ca 19-9	59	ND	ND	4608	ND
Treatment dates (dd/mm/yyyy)	Start date	06/01/2012	04/04/2012	07/03/2012	22/02/2012	15/02/2012
	End date	26/09/2012	01/08/2012	11/07/2012	11/05/2012	08/06/2012

285 **Table 3:** Patient characteristics prior to treatment. ND denotes non-discernable
 286 values. Start and end date of treatment are also stated.

287

288 **Control group**

289

290 Taking into account the guidelines for gemcitabine treatment, it can be deduced that
 291 the more treatment cycles the patient can undergo, the longer the patient can be
 292 considered healthy; hence the more effective the treatment. Once the patient surpasses
 293 a Level 2 in the ECOG performance status guidelines, they would no longer receive
 294 treatment; this would accordingly define the end of the healthy and ambulatory
 295 period. Our control group consisted of 80 patients from 2009-2011 with histology

296 showing pancreatic adenocarcinoma (matching the same criteria as our patients).
297 These patients received the identical chemotherapy treatment (in accordance to
298 Gemzar guidelines [50]) at Haukeland University Hospital, Bergen, Norway. The
299 control treatments were also discontinued once they surpassed and ECOG
300 performance grade of 2 or their blood counts dropped below the chemotherapy
301 guidelines. Patients who received a different treatment were excluded from the control
302 group. The data was accessed through the internal hospital medical system. The same
303 anonymous data will be available on the Norwegian national cancer registry.

304

305 **Ethical Considerations**

306

307 All experiments were performed with approval from the regional ethics committee
308 under reference number 2011/1601/REK vest.

309

310 **Results and discussion**

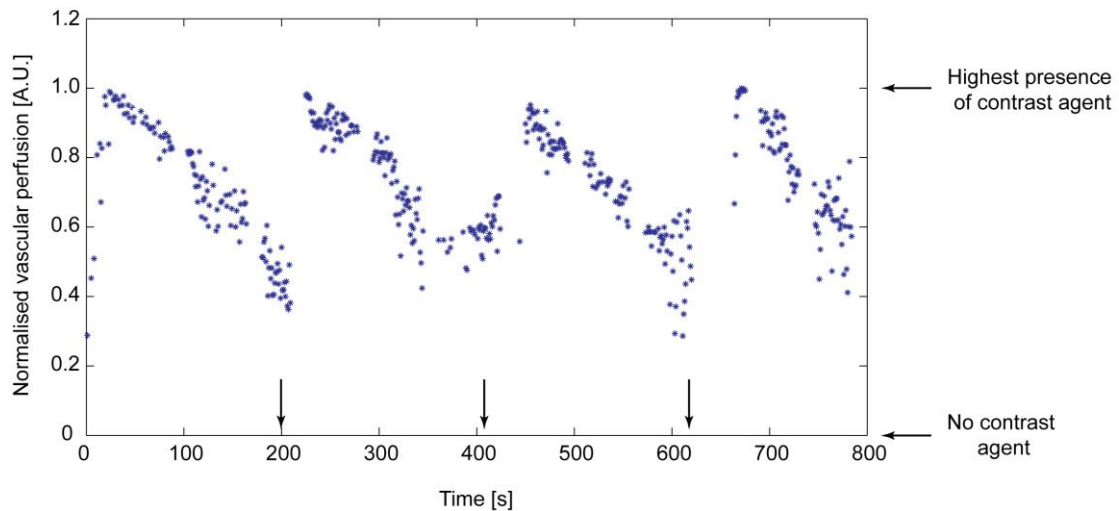
311 The beam characterisation showed that the clinical scanner took into account the
312 attenuation of soft tissue when varying the focal depth. This allowed for a good
313 prediction of the ultrasound profile *in-situ* and easy manipulation of the ultrasound
314 intensity and positioning. The “active” area that we assume enhances the
315 chemotherapy effect was long and wide in all cases independent of depth, surpassing
316 the tumour size, allowing a maximum flexibility on treatment area. It has be assumed
317 that there are some fluctuations in the sound field pressures due to tissue property
318 variations, but this should not drastically change the sound field in our case, as
319 acoustic propagation was only though soft tissue. Taking into account the vast range
320 of ultrasound intensities used to induce sonoporation, as seen in literature, we assume

321 that sonoporation may be occurring at lower or higher acoustic pressures independent
322 of the varying attenuation of tissue. A benefit of using a clinical probe is also that due
323 to the synthetic aperture, objects obscuring the field of view do not affect the beam
324 formation in other areas; hence we can predict the ultrasound dose delivered to our
325 target area.

326 The image generated using our customised treatment settings allowed easy
327 identification of both microbubbles and tumours. Figure 4A shows clear signs of
328 microbubble presence in the tumour vasculature and surrounding tissue. Figure 4B
329 shows the dimensions of a pancreatic tumour indicating the ease of detecting and
330 aligning the probe to the tumour using the modified settings.

331 Figure 7 shows the normalised perfusion curve where the arrows indicate the contrast
332 injection time, as measured by the clinical scanner during the first 13 minutes of
333 ultrasound and microbubble treatment. A pseudo-sinusoidal perfusion curve can be
334 seen. Throughout the whole treatment we can see that there are always microbubbles
335 present. By using this pseudo-continuous method we can ensure that there are always
336 microbubbles present without the added complexity of continuous infusion
337 equipment.

338



339

340 **Figure 7:** Normalised microbubble presence in tumour locality during the first 800 s
 341 of treatment. Arrows indicate contrast injection time.

342

343 Our control group, treated with the same chemotherapeutic protocol, received an
 344 average of 9 ± 6 treatment cycles. To date all patients participating in this trial have
 345 already surpassed this indicating the potential benefit of our combined treatment on a
 346 clinical scale with minimal changes to chemotherapy protocols. The patients enrolled
 347 in this clinical pilot study received an average of 16 ± 7 treatment cycles.

348 Figure 8 and Table 3 show the effect of our combined treatment on the tumour size.

349 After 8 weeks two patients showed a tumour diameter reduction. Patient 1 had a
 350 temporary tumour reduction from 4.0 cm to 3.1 cm. The next CT image was taken 24
 351 weeks later and showed a growth to 4.6 cm; an increase of 15% from the original
 352 tumour size after 32 weeks of treatment. In patient 2, the treatment resulted in a
 353 continuous tumour reduction over 16 weeks, a very rare response from chemotherapy
 354 alone. As a result of his increased health, after 10 treatment cycles, he was removed
 355 from the clinical trial to undergo radiation therapy. As this patient was removed from
 356 the trial due to the success of the treatment, a lower number of total and average
 357 treatments was seen, reducing the apparent effectiveness of the treatment as a whole.

358 It should be noted that none of the patients in the control group stopped treatment due
359 to its success but on the contrary, due to their deterioration.

360 Two patients showed slow tumour growth from the 8th week onwards (patient 3 and
361 patient 4). Patient 5 also had a biopsy verified primary tumour in the pancreas. This
362 was surgically removed but re-occurred with a small tumour in the operation sight and
363 a large metastasis. This indicated that the tumour was at a late stage of development
364 hence a limited response could be expected from the chemotherapeutic. Nevertheless,
365 this patient was also able to receive 11 cycles of treatment.

366 As pancreatic cancer is such an aggressive form of cancer it is very uncommon to see
367 any decrease in tumour growth from chemotherapy. Our aim was to improve quality
368 of life, to extend the healthy period of life, and conclusively extend the patients
369 survival. If the patient was “healthy” enough (well-defined state in both groups,
370 ECOG performance status 0-2 [51]), they would be able to receive treatment for a
371 longer period. In fact, as long they are ambulatory and capable of all self-care they are
372 able to receive the treatment. Seeing a decrease in the primary tumour size was an
373 added benefit to the increased number of treatment cycles and thereby the anticipated
374 survival.

375

376

377

378

379

380

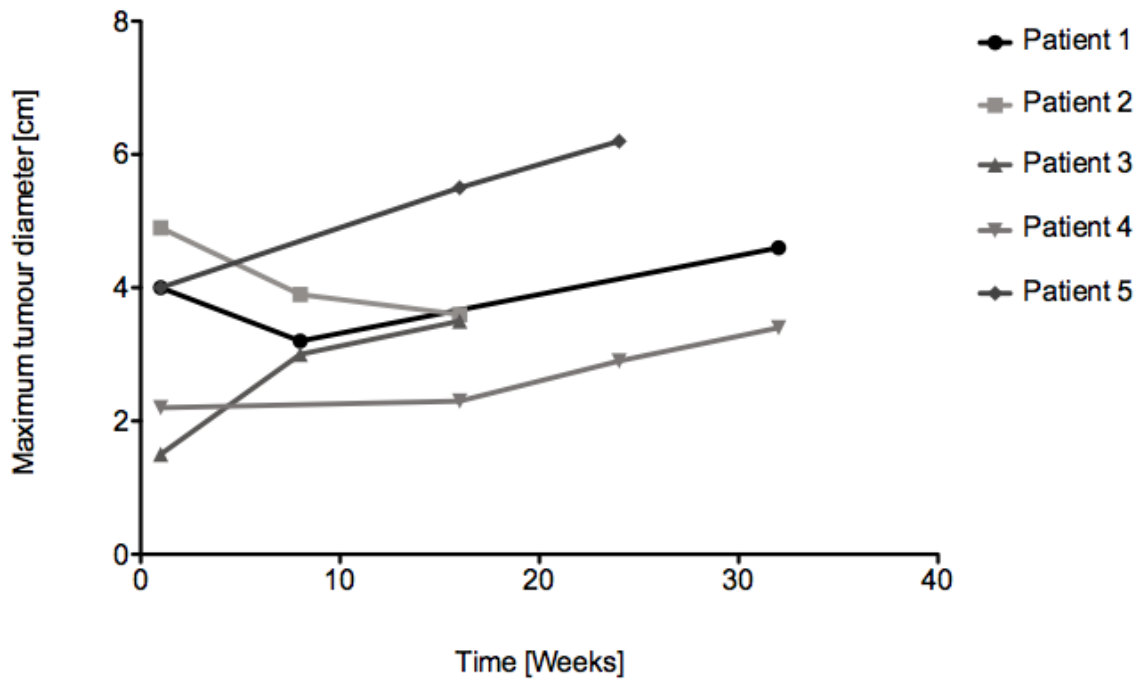
381

382

Patient	Maximum tumour diameter (cm)					Total number of cycles
	Inclusion day	Week 8	Week 16	Week 24	Week 32	
1	4.0	3.1	-	-	4.6	27
2	4.9	3.9	3.6	-	-	10
3	1.5	3.0	3.5	-	-	11
4	2.2	-	2.3	2.9	3.4	16
5	4.0	-	5.5	6.2	-	16

Table 4: Maximum tumour diameter as measured from CT images. Empty values denote skipped CT scans.

383



384

385 **Figure 8:** Change in tumour diameter over time measured from CT images in patients

386

with pancreatic malignancy.

387

388 The addition of the sonoporation procedure following the standard chemotherapeutic
389 protocol did not add any discomfort to the patients. All patients were very relaxed
390 during the treatment to a state where they could comfortably sleep throughout the
391 whole treatment.

392 In this study we also aimed to show that it is possible to induce sonoporation in the
393 clinic using existing commercial equipment, whilst fitting in the current safety
394 regulations for the use of diagnostic ultrasound. In our previous work we showed that
395 a duty cycle of 40% was ideal for sonoporation [7, 23]. Here we are using a duty
396 cycle of 1%; hence expecting a small effect of sonoporation. There are many ways to
397 improve this method of therapy such as by increasing the duty cycle from 1% to 40%
398 and introducing targeted microbubbles that could attach to specific cancer cells [40].

399 The efficacy of our combined treatment should be compared to the efficacy of the
400 current golden standard, the chemotherapeutic gemcitabine alone, where the viability
401 of the patient has been extended by approximately 1 month [3, 4].

402 **Conclusion**

403 Using a clinical diagnostic scanner for therapeutic purposes allows accurate acoustic
404 field alignment ensuring that the desired ultrasound dose reaches the target area. This
405 configuration allows simultaneous visualisation of the microbubbles present whilst
406 treating the pancreatic tumour. In this pilot study, we saw an extended treatment
407 period when comparing to the control group. Furthermore, we did not notice any
408 adverse side effects. Combined ultrasound, microbubble and chemotherapeutic
409 treatment could pave the way for a novel enhanced drug delivery pathways.

410

411

412

413 **Acknowledgements**

414 This study has been supported by funds from the Norwegian Cancer Society (NCS)
415 and MedViz (<http://medviz.uib.no/>), an interdisciplinary research cluster from
416 Haukeland University Hospital, University of Bergen and Christian Michelsen
417 Research AS. We would like to thank Dr. Martin Biermann, Dr. Tormod Bjårnes, Dr.
418 Bjørn Tore Gjertsen, Dr. Anders Molven and Dr. Halfdan Sørbye for their support
419 throughout this project.

420

421

423

- 424 [1] World Health Organization. (2012). *World Health Statistics*. Available:
425 [http://www.who.int/gho/publications/world_health_statistics/2012/en/index.ht](http://www.who.int/gho/publications/world_health_statistics/2012/en/index.html)
426 [ml](http://www.who.int/gho/publications/world_health_statistics/2012/en/index.html)
- 427 [2] D. Hariharan, A. Saied, and H. M. Kocher, "Analysis of mortality rates for
428 pancreatic cancer across the world," *HPB (Oxford)*, vol. **10**, pp. 58-62, (2008).
- 429 [3] J. P. Neoptolemos, J. A. Dunn, D. D. Stocken, J. Almond, K. Link, H. Beger,
430 C. Bassi, M. Falconi, P. Pederzoli, C. Dervenis, L. Fernandez-Cruz, F. Lacaine,
431 A. Pap, D. Spooner, D. J. Kerr, H. Friess, M. W. Buchler, and C. European
432 Study Group for Pancreatic, "Adjuvant chemoradiotherapy and chemotherapy
433 in resectable pancreatic cancer: a randomised controlled trial," *Lancet*, vol.
434 **358**, pp. 1576-1585, (2001).
- 435 [4] J. P. Neoptolemos, D. D. Stocken, H. Friess, C. Bassi, J. A. Dunn, H. Hickey,
436 H. Beger, L. Fernandez-Cruz, C. Dervenis, F. Lacaine, M. Falconi, P.
437 Pederzoli, A. Pap, D. Spooner, D. J. Kerr, M. W. Buchler, and C. European
438 Study Group for Pancreatic, "A randomized trial of chemoradiotherapy and
439 chemotherapy after resection of pancreatic cancer," *N Engl J Med*, vol. **350**,
440 pp. 1200-1210, (2004).
- 441 [5] S. Bao, B. D. Thrall, and D. L. Miller, "Transfection of a reporter plasmid into
442 cultured cells by sonoporation in vitro," *Ultrasound Med. Biol.*, vol. **23**, pp.
443 953-959, (1997).
- 444 [6] A. van Wamel, K. Kooiman, M. Hartevelde, M. Emmer, F. J. ten Cate, M.
445 Versluis, and N. de Jong, "Vibrating microbubbles poking individual cells:
446 drug transfer into cells via sonoporation," *J. Control. Release*, vol. **112**, pp.
447 149-155, (2006).
- 448 [7] A. Delalande, S. Kotopoulis, T. Rovers, C. Pichon, and M. Postema,
449 "Sonoporation at a low mechanical index," *Bub. Sci. Eng. Tech.*, vol. **3**, pp. 3-
450 11, (2011).
- 451 [8] M. Postema, S. Kotopoulis, A. Delalande, and O. H. Gilja, "Sonoporation:
452 Why microbubbles create pores," *Ultraschall in Med.*, vol. **33**, pp. 97-98,
453 (2012).
- 454 [9] N. G. Lee, J. L. Berry, T. C. Lee, A. T. Wang, S. Honowitz, A. L. Murphree,
455 N. Varshney, D. R. Hinton, and A. A. Fawzi, "Sonoporation enhances
456 chemotherapeutic efficacy in retinoblastoma cells in vitro," *Invest Ophthalmol*
457 *Vis Sci*, vol. **52**, pp. 3868-3873, (2011).
- 458 [10] C. X. Deng, F. Sieling, H. Pan, and J. Cui, "Ultrasound-induced cell
459 membrane porosity," *Ultrasound Med Biol*, vol. **30**, pp. 519-526, (2004).
- 460 [11] R. K. Schlicher, H. Radhakrishna, T. P. Tolentino, R. P. Apkarian, V.
461 Zarnitsyn, and M. R. Prausnitz, "Mechanism of intracellular delivery by
462 acoustic cavitation," *Ultrasound Med Biol*, vol. **32**, pp. 915-924, (2006).
- 463 [12] Y. Z. Zhao, Y. K. Luo, C. T. Lu, J. F. Xu, J. Tang, M. Zhang, Y. Zhang, and H.
464 D. Liang, "Phospholipids-based microbubbles sonoporation pore size and
465 reseal of cell membrane cultured in vitro," *J Drug Target*, vol. **16**, pp. 18-25,
466 (2008).
- 467 [13] M. Postema and O. H. Gilja, "Ultrasound-directed drug delivery," *Curr.*
468 *Pharm. Biotechnol.*, vol. **8**, pp. 355-361, (2007).

- 469 [14] M. Postema, O. H. Gilja, and A. van Wamel, "CEUS and sonoporation," in
470 *Fundamentals of Medical Ultrasonics*, M. Postema, Ed., London: Spon press,
471 2011, pp. 205-217.
- 472 [15] M. Postema, S. Kotopoulis, A. Delalande, and O. H. Gilja, "Ultrasound-guided
473 delivery and sonoporation," in *Ultrasound in Gastroenterology. 10-years*
474 *aniversary of National Center for Ultrasound in Gastroenterology*, 2011, pp.
475 57-59.
- 476 [16] J. M. Escoffre, A. Novell, J. Piron, A. Zeghimi, A. Doinikov, and A. Bouakaz,
477 "Microbubble attenuation and destruction: are they involved in sonoporation
478 efficiency?," *IEEE Trans Ultrason Ferroelectr Freq Control*, vol. **60**, pp. 46-
479 52, (2013).
- 480 [17] D. L. Miller and C. Dou, "Membrane damage thresholds for 1- to 10-MHz
481 pulsed ultrasound exposure of phagocytic cells loaded with contrast agent gas
482 bodies in vitro," *Ultrasound Med. Biol.*, vol. **30**, pp. 973-977, (2004).
- 483 [18] D. L. Miller and C. Dou, "Membrane damage thresholds for pulsed or
484 continuous ultrasound in phagocytic cells loaded with contrast agent gas
485 bodies," *Ultrasound Med. Biol.*, vol. **30**, pp. 405-411, (2004).
- 486 [19] D. L. Miller, C. Dou, and J. Song, "DNA transfer and cell killing in
487 epidermoid cells by diagnostic ultrasound activation of contrast agent gas
488 bodies in vitro," *Ultrasound Med. Biol.*, vol. **29**, pp. 601-607, (2003).
- 489 [20] D. L. Miller and J. Quddus, "Sonoporation of monolayer cells by diagnostic
490 ultrasound activation of contrast-agent gas bodies," *Ultrasound Med. Biol.*, vol.
491 **26**, pp. 661-667, (2000).
- 492 [21] M. W. Miller, "Gene transfection and drug delivery," *Ultrasound Med. Biol.*,
493 vol. **26**, pp. S59-S62, (2000).
- 494 [22] K. Kooiman, M. Harteveld, A. F. W. van der Steen, and N. de Jong,
495 "Sonoporation of endothelial cells by vibrating targeted microbubbles," *J.*
496 *Control Release*, vol. **154**, pp. 35-41, (2011).
- 497 [23] A. Delalande, A. Bouakaz, G. Renault, F. Tabareau, S. Kotopoulis, P. Midoux,
498 B. Arbeille, R. Uzbekov, S. Chakravarti, M. Postema, and C. Pichon,
499 "Ultrasound and microbubble-assisted gene delivery in Achilles tendons: long
500 lasting gene expression and restoration of fibromodulin KO phenotype," *J*
501 *Control Release*, vol. **156**, pp. 223-230, (2011).
- 502 [24] S. M. Nejad, S. H. R. Hosseini, H. Akiyama, and K. Tachibana, "Optical
503 observation of cell sonoporation with low intensity ultrasound," *Biochemical*
504 *and Biophysical Research Communications*, vol. **413**, pp. 218-223, (2011).
- 505 [25] F. Yang, N. Gu, D. Chen, X. Xi, D. Zhang, Y. Li, and J. Wu, "Experimental
506 study on cell self-sealing during sonoporation," *J Control Release*, vol. **131**,
507 pp. 205-210, (2008).
- 508 [26] Y. Qiu, C. Zhang, J. Tu, and D. Zhang, "Microbubble-induced sonoporation
509 involved in ultrasound-mediated DNA transfection in vitro at low acoustic
510 pressures," *Journal of Biomechanics*, vol. **45**, pp. 1339-1345, (2012).
- 511 [27] M. Matsuo, K. Yamaguchi, L. B. Feril, Jr., H. Endo, K. Ogawa, K. Tachibana,
512 and J. Nakayama, "Synergistic inhibition of malignant melanoma proliferation
513 by melphalan combined with ultrasound and microbubbles," *Ultrason*
514 *Sonochem*, vol. **18**, pp. 1218-1224, (2011).
- 515 [28] N. Lamanauskas, A. Novell, J. M. Escoffre, M. Venslauskas, S. Satkauskas,
516 and A. Bouakaz, "Bleomycin delivery into cancer cells in vitro with
517 ultrasound and SonoVue® or BR14® microbubbles.," *J Drug Target*, vol. **1**, p.
518 [Epub ahead of print], (2013).

- 519 [29] Y. Watanabe, A. Aoi, S. Horie, N. Tomita, S. Mori, H. Morikawa, Y.
520 Matsumura, G. Vassaux, and T. Kodama, "Low-intensity ultrasound and
521 microbubbles enhance the antitumor effect of cisplatin," *Cancer Sci*, vol. **99**,
522 pp. 2525-2531, (2008).
- 523 [30] J. Wu, J. Pepe, and M. Rincon, "Sonoporation, anti-cancer drug and antibody
524 delivery using ultrasound," *Ultrasonics*, vol. **44**, pp. E21-E25, (2006).
- 525 [31] C. Y. Lai, C. H. Wu, C. C.C., and P. C. Li, "Quantitative relations of acoustic
526 inertial cavitation with sonoporation and cell viability," *Ultrasound Med. Biol.*,
527 vol. **32**, pp. 1931-1941, (2006).
- 528 [32] D. M. Hallow, A. D. Mahajan, T. E. McCutchen, and M. R. Prausnitz,
529 "Measurement and correlation of acoustic cavitation with cellular bioeffects,"
530 *Ultrasound Med. Biol.*, vol. **32**, pp. 1111-1122, (2006).
- 531 [33] M. M. Forbes, R. L. Steinberg, and W. D. O'Brien, "Examination of Inertial
532 Cavitation of Optison in Producing Sonoporation of Chinese Hamster Ovary
533 Cells," *Ultrasound in Medicine and Biology*, vol. **34**, pp. 2009-2018, (2008).
- 534 [34] J. L. Tlaxca, C. R. Anderson, A. L. Klibanov, B. Lowrey, J. A. Hossack, J. S.
535 Alexander, M. B. Lawrence, and J. J. Rychak, "Analysis of in vitro
536 Transfection by Sonoporation Using Cationic and Neutral Microbubbles,"
537 *Ultrasound Med Biol*, vol. **36**, pp. 1907-1918, (2010).
- 538 [35] C. D. Ohl and B. Wolfrum, "Detachment and sonoporation of adherent HeLa-
539 cells by shock wave-induced cavitation," *Biochimica Et Biophysica Acta-
540 General Subjects*, vol. **1624**, pp. 131-138, (2003).
- 541 [36] D. L. Miller and C. Y. Dou, "Induction of Apoptosis in Sonoporation and
542 Ultrasonic Gene Transfer," *Ultrasound in Medicine and Biology*, vol. **35**, pp.
543 144-154, (2009).
- 544 [37] M. Postema and O. H. Gilja, "Jetting does not cause sonoporation," *Biomed.
545 Eng.*, vol. **55**, pp. S19-S20, (2010).
- 546 [38] B. Geers, H. Dewitte, S. C. De Smedt, and I. Lentacker, "Crucial factors and
547 emerging concepts in ultrasound-triggered drug delivery," *J Control Release*,
548 vol. **164**, pp. 248-255, (2012).
- 549 [39] F. G. Erchinger, G. Dimcevski, T. Engjom, and O. H. Gilja, "Transabdominal
550 ultrasonography of the pancreas: basic and new aspects," *Imaging Med.*, vol. **3**,
551 pp. 412-422, (2011).
- 552 [40] M. Postema and O. H. Gilja, "Contrast-enhanced and targeted ultrasound,"
553 *World J. Gastroenterol.*, vol. **17**, pp. 28-41, (2011).
- 554 [41] F. Piscaglia, C. Nolsoe, C. F. Dietrich, D. O. Cosgrove, O. H. Gilja, M.
555 Bachmann Nielsen, T. Albrecht, L. Barozzi, M. Bertolotto, O. Catalano, M.
556 Claudon, D. A. Clevert, J. M. Correas, M. D'Onofrio, F. M. Drudi, J. Eyding,
557 M. Giovannini, M. Hocke, A. Ignee, E. M. Jung, A. S. Klausner, N. Lassau, E.
558 Leen, G. Mathis, A. Saftoiu, G. Seidel, P. S. Sidhu, G. ter Haar, D.
559 Timmerman, and H. P. Weskott, "The EFSUMB Guidelines and
560 Recommendations on the Clinical Practice of Contrast Enhanced Ultrasound
561 (CEUS): update 2011 on non-hepatic applications," *Ultraschall in Med.*, vol.
562 **33**, pp. 33-59, (2012).
- 563 [42] M. Postema, *Fundamentals of medical ultrasonics*. Milton Park, Abingdon,
564 Oxon ; New York: Spon Press, 2011.
- 565 [43] B. Gerold, S. Kotopoulis, M. C., D. McGloin, M. Postema, and P. Prentice,
566 "Laser-nucleated acoustic cavitation in focused ultrasound," *Rev. Sci. Instrum.*,
567 vol. **82**, p. 044908, (2011).

- 568 [44] U.S. Department of Health and Human Services. Food and Drug
569 Administration, "Information for Manufacturers Seeking Marketing Clearance
570 of Diagnostic Ultrasound Systems and Transducers," 2008.
- 571 [45] International Electrotechnical Commission, "Ultrasonics - Hydrophones - Part
572 2: Calibration for ultrasonic fields up to 40 MHz," 2013.
- 573 [46] J. A. Jensen, S. I. Nikolov, K. L. Gammelmark, and M. H. Pedersen,
574 "Synthetic aperture ultrasound imaging," *Ultrasonics*, vol. **44 Suppl 1**, pp. e5-
575 15, (2006).
- 576 [47] E. Quaia, "Microbubble ultrasound contrast agents: an update," *European
577 Radiology*, vol. **17**, pp. 1995-2008, (2007).
- 578 [48] British Medical Ultrasound Society, *Guidelines for the safe use of diagnostic
579 ultrasound equipment*, 2000.
- 580 [49] S. B. Barnett, G. R. Ter Haar, M. C. Ziskin, H. D. Rott, F. A. Duck, and K.
581 Maeda, "International recommendations and guidelines for the safe use of
582 diagnostic ultrasound in medicine," *Ultrasound Med Biol*, vol. **26**, pp. 355-366,
583 (2000).
- 584 [50] Eli Lilly and Company. (2010). *Highlights of prescribing information -
585 Gemzar*. Available: <http://pi.lilly.com/us/gemzar.pdf>
- 586 [51] M. M. Oken, R. H. Creech, D. C. Tormey, J. Horton, T. E. Davis, E. T.
587 Mcfadden, and P. P. Carbone, "Toxicity and Response Criteria of the Eastern-
588 Cooperative-Oncology-Group," *American Journal of Clinical Oncology-
589 Cancer Clinical Trials*, vol. **5**, pp. 649-655, (1982).
- 590 [52] E. A. Eisenhauer, P. Therasse, J. Bogaerts, L. H. Schwartz, D. Sargent, R.
591 Ford, J. Dancey, S. Arbuck, S. Gwyther, M. Mooney, L. Rubinstein, L.
592 Shankar, L. Dodd, R. Kaplan, D. Lacombe, and J. Verweij, "New response
593 evaluation criteria in solid tumours: Revised RECIST guideline (version 1.1),"
594 *European Journal of Cancer*, vol. **45**, pp. 228-247, (2009).
- 595 [53] S. A. Sohaib, B. Turner, J. A. Hanson, M. Farquharson, R. T. Oliver, and R. H.
596 Reznek, "CT assessment of tumour response to treatment: comparison of
597 linear, cross-sectional and volumetric measures of tumour size," *Br J Radiol*,
598 vol. **73**, pp. 1178-1184, (2000).

599

600

601